Journal of Clinical and Translational Hepatology **2022** vol. 10(4) | 680–691
DOI: 10.14218/JCTH.2021.00511

Original Article

CircTUBD1 Regulates Radiation-induced Liver Fibrosis Response via a circTUBD1/micro-203a-3p/Smad3 Positive Feedback Loop

Hao Niu[1#], Li Zhang[1#], Biao Wang[1], Guang-Cong Zhang[2], Juan Liu[1], Zhi-Feng Wu[1], Shi-Suo Du[1,3] and Zhao-Chong Zeng[1,3*]

[1]Department of Radiation Oncology, Zhongshan Hospital, Fudan University, Shanghai, China; [2]Department of Gastroenterology and Hepatology, Zhongshan Hospital, Fudan University, Shanghai, China; [3]Cancer Center, Zhongshan Hospital, Fudan University, Shanghai, China

Received: 10 November 2021 | **Revised:** 19 January 2022 | **Accepted:** 20 January 2022 | **Published:** 28 February 2022

Abstract

Background and Aims: Radiation-induced liver fibrosis (RILF), delayed damage to the liver (post-irradiation) remains a major challenge for the radiotherapy of liver malignancies. This study investigated the potential function and mechanism of circTUBD1 in the development of RILF. ***Methods:*** By using a dual luciferase assay, RNA pull-down assays, RNA sequencing, chromatin immunoprecipitation (known as ChIP) assays, and a series of gain- or loss-of-function experiments, it was found that circTUBD1 regulated the activation and fibrosis response of LX-2 cells induced by irradiation via a circTUBD1/micro-203a-3p/Smad3 positive feedback loop in a 3D system. ***Results:*** Knockdown of circTUBD1 not only reduced the expression of α-SMA, as a marker of LX-2 cell activation, but also significantly decreased the levels of hepatic fibrosis molecules, collagen type I alpha 1 (COL1A1), collagen type III alpha 1 (COL3A1), and connective tissue growth factor (CTGF) in a three-dimensional (3D) culture system and RILF model *in vivo*. Notably, knockdown of circTUBD1 alleviated early liver fibrosis induced by irradiation in mice models. ***Conclusions:*** This study is the first to reveal the mechanism and role of circTUBD1 in RILF via a circTUBD1/micro-203a-3p/Smad3 feedback loop, which provides a novel therapeutic strategy for relieving the progression of RILF.

Citation of this article: Niu H, Zhang L, Wang B, Zhang GC, Liu J, Wu ZF, *et al*. CircTUBD1 Regulates Radiation-induced Liver Fibrosis Response via a circTUBD1/micro-203a-3p/Smad3 Positive Feedback Loop. J Clin Transl Hepatol 2022;10(4):680–691. doi: 10.14218/JCTH.2021.00511.

Keywords: circRNA; Radiation-induced liver fibrosis; Three-dimensional; Collagens; LX-2.

Abbreviations: 2D, two-dimensional; 3D, three-dimensional; COL1A1, collagen type I alpha 1; COL3A1, collagen type III alpha 1; CTGF, connective tissue growth factor; DAPI, diamidino-2-phenylindole; HSCs, hepatic stellate cells; RILF, radiation-induced liver fibrosis.

#Contributed equally to this work.

***Correspondence to:** Zhao-Chong Zeng, Department of Radiation Oncology, Zhongshan Hospital, Fudan University, 180 Feng Lin Road, Shanghai 200032, China. ORCID: https://orcid.org/0000-0003-4330-3688. Tel: +86-21-64041990, Fax: +86-21-6404-8472, E-mail: zeng.zhaochong@zs-hospital.sh.cn

Introduction

Radiotherapy is one of the most important nonsurgical treatments of liver malignancies[1] such as hepatocellular carcinoma and intrahepatic cholangiocarcinoma. However, the efficacy of radiotherapy for liver malignancy is severely limited by radiation-induced liver fibrosis (RILF),[2] which prevents re-irradiation or irradiation dose escalation for additional treatment of the cancer.[1–4] It cannot be ignored that patients with liver dysfunction have a decreased tolerance to radiation and are more likely to develop RILF after completion of radiotherapy.[2,5,6] Therefore, it is necessary to thoroughly clarify the central mechanisms underlying RILF and find suitable interventions to prevent or alleviate RILF occurrence and development.

However, research progress in RILF remains slow and no efficient therapies are available. One of the major obstacles is the lack of a stable fibrosis model induced by irradiation *in vitro*.[7] Hepatic stellate cells (HSCs) are the main fibrosis cell type of liver fibrosis.[8] However, human primary HSCs are difficult to culture because they have limited proliferation capacity. The two-dimensional (2D) culture model's rapid dedifferentiation limits observation of the long-term cell phenotypes of chronic liver diseases, such as hepatotoxicity or fibrosis. Thus, it is imperative to develop new *in vitro* systems for maintaining quiescent LX-2 cells during prolonged periods of culture. A 3D culture system has recently gained much attention as a reliable system *in vitro* for studying various molecular and screening therapeutic drugs.[7,9,10] Pingitore *et al*. established multilineage 3D spheroids as a model of liver steatosis and reported that LX-2 cells facilitate the compactness of 3D spheroids.[9] In addition, the 3D model system is more similar to *in vivo* conditions, which makes it a realistic system for *in vitro* translation studies.[10,11] These studies suggested that 3D cultures have potential as an *in vitro* model to explore mechanisms involved in chronic liver diseases.[7,9,11]

Increasing evidence shows that small RNA molecules have significant roles in the regulation of a variety of biological processes.[12] In addition, circRNAs characteristically have tissue-specific expression patterns[13] that indicate they have a potential role in the diagnosis and treatment of disease. It was reported that circ-10720 serves as a biomarker of hepatocellular carcinoma and is positively correlated with poor prognosis in hepatocellular carcinoma.[13] Hsa_circ_0070963 inhib-

its liver fibrosis by regulation of miR-223-3p and LEMD3.[14] The findings suggest that targeting circRNAs is a promising therapeutic strategy. However, the expression and function of circRNAs in RILF remain largely unexamined. Because conventional 2D cell culture is sensitive to irradiation, it restricts observation of the chronic phenotype of liver fibrosis induced by high-dose irradiation. To study RILF, we successfully established a 3D spheroid model of LX-2 cells, which greatly facilitated this research. To examine the mechanism of activation and fibrogenic response of LX-2 cells to irradiation, a circRNA microarray was used to screen differentially expressed circRNAs in irradiated and nonirradiated LX-2 cells in our previous study.[15] Among the significantly different circRNAs, circTUBD1 (hsa_circ_0044897) caught our attention because it was significantly upregulated, and its change was consistent with the activation of LX-2 cells. In this study, its role and regulation mechanism were further investigated in a 3D spheroid model of human HSCs LX-2 cells and in RILF mice models.

Methods

3D spheroid culture

LX-2 cells were purchased from the Shanghai Academy of Life Sciences (Shanghai, China) and cultured in Dulbecco's Modified Eagle Medium (HyClone Laboratories, Logan, UT, USA). LX-2 cells were seeded into ultra low-attachment 96-well plates (Corning, Corning, NY, USA) at 3,000 viable cells per well in 200 μL specific culture medium with 2% fetal bovine serum (FBS), 100 U/mL penicillin, and 100 μg/mL streptomycin. The spheroids were sufficiently compact at 3 days after seeding, and 50% of the medium was exchanged daily with fresh medium. Spheroids were transferred to spinner flasks and maintained on a constant temperature cell shaker with stirring at 50 rpm.

Cell irradiation with X-rays

To minimize cell activation, the cells were cultured for 3–5 generations after irradiation. LX-2 cells were irradiated with a single dose of 8 Gy X-rays, a photon beam energy of 8 MV, and at a dose rate of 300 cGy/min using an ONCORTM linear accelerator (Siemens, Munich, Germany). The distance between the cell plates and the X-ray source was 100 cm. The cells were collected at the indicated times for subsequent experiments.

Cell viability assay

To measure cell viability, a CellTiter-Glo Luminescent Cell Viability Assay kit (Promega, Madison, WI, USA) was used following the manufacturer's instructions to measure ATP content. Briefly, 50 μL reagent was added to each sample well. After disruption of spheroids by pipetting, the plate was incubated at room temperature for 20 min in the dark. Then, the plate was placed in a SpectraMax i3 (Molecular Devices, San Jose, CA, USA) counter and luminescence was measured with SoftMax Pro 6.3 software (Molecular Devices).

Immunofluorescence

Briefly, 3D spheroidal cells were fixed with 8% paraformaldehyde for 12 h, embedded in OCT Cryomount, and then sectioned at 8 μm. The sections were permeabilized with 0.5% Triton X-100, blocked with 10% FBS, and then incubated with primary antibodies against α-SMA, COL1A1, COL3A1, CTGF (Cell Signaling Technology, Danvers, MA, USA) for 60 min at 37°C. All antibodies were diluted in 0.2% (w/v) bovine serum albumen in phosphate buffered saline. Sections were then probed with a Cy3-conjugated goat antimouse or antirabbit IgG secondary antibody for 30 min at 37°C. Nuclei were stained with antifade mounting medium containing diamidino-2-phenylindole (DAPI) (Beyotime Institute of Biotechnology, Shanghai, China). Images were obtained by fluorescence microscopy (model BZ 700; Keyence, Osaka, Japan).

RNA pull-down assay

RNA pull-down assays were performed following the manufacturer's instructions. Briefly, for circTUBD1 to pull down endogenous miR-203a-3p, a biotin-coupled probe was designed to bind to the junction sites of circTUBD1, and a negative probe was used as a control. Biotin-circTUBD1 and its negative probe were incubated with 600 μg streptavidin magnetic beads (Life Technologies, Carlsbad, CA, USA) to form a biotin-coupled RNA complex. Total RNA was extracted from 2×10^7 LX-2 cells, and 200 μg total RNA was incubated with the biotin-coupled RNA complex. Bound RNAs were evaluated by qRT-PCR. The same method was used for biotin-miR-203a-3p mimics to pull down endogenous circTUBD1. The circTUBD1 probe, miR-203a-3p probe, and the corresponding negative control probes are listed in Supplementary Table 1.

RNA sequencing analysis

LX-2 cells transfected with small interfering RNA targeting circTUBD1 and its negative control were treated with 8 Gy X-rays. After irradiation for 72 h, LX-2 cells were collected for RNA sequencing. Transcriptome sequencing and bioinformatics analysis was performed with an Illumina HiSeq2500 instrument at Shanghai Majorbio Biopharm Technology Co. Ltd. (Shanghai, China).

ChIP assay

ChIP assays were performed following the manufacturer's protocol using the Magna Ch-IP G Assay kit (EMD Millipore, Temecula, CA, USA). Briefly, cells were cross-linked with 1% formaldehyde for 10 m at room temperature, and quenched with 0.25 mol/L glycine. The cell pellet was resuspended in lysis buffer and incubated on ice for 15 min. The pellet was resuspended in nuclear lysis buffer. Effective sonication was confirmed by bioanalyzer analysis. The chromatin fraction was incubated with an anti-SMAD3 mAb (1:100) overnight at 4°C. The protein/DNA cross links were reversed to obtain free DNA, and after cross links were reversed, the purified DNA was detected and amplified by PCR.

RILF model establishment and studies

Male C57/B6J mice (6 weeks of age) were purchased from Shanghai Laboratory Animal Co. Ltd (SLAC, Shanghai, China) and maintained in pathogen-free conditions. Mice were randomly allocated to four groups of 12 each. The RILF model was constructed by irradiating the left liver with 30 Gy with five fractions, 6 Gy/per week. After 4 weeks of irradiation, adenovirus (Ad-cirTUBD1-NC, Ad-sh1-circTUBD1 and Ad-sh2-circTUBD1) were administrated through the tail vein at a titer of 5×10^8 pfu/mouse, once/week, three times. After 6 months of irradiation, the mice were killed by meth-

ods following the regulations of Animal Ethics Committee of Zhongshan Hospital, Fudan University. Liver tissue was collected for hematoxylin and eosin, Masson-trichrome, and Sirius red staining, immunohistochemistry (IHC), western blotting, and qRT-PCR assays.

Statistical analysis

Statistical analysis was performed with GraphPad Prism 8 and SPSS v. 26.0.0.2. Results were compared by one-way analysis of variance, followed by Student's *t*-test for unpaired observations or Bonferroni's correction for multiple comparisons. A p-value of <0.05 was considered significant. Results were reported as means ± standard error of the means.

Supplementary Methods

For details about other methods, please refer to Supplementary File 1.

Results

Irradiation-induced human HSC activation and fibrosis response

To detect the effect of irradiation on the viability of the LX-2 cell spheroids, ATP levels of spheroids irradiated with 8 Gy X-rays were measured. Spheroid viability increased within 3 days before irradiation and decreased after irradiation, but maintained higher levels until 4 days after irradiation compared with 2D culture (Fig. 1A, B). Compared with 12 h after irradiation, α-SMA began to increase significantly at 24 h and remained at a high level. Fibrotic indicators of HSCs, such as COL1A1, COL3A1, and CTGF, were not significantly increased within 24 h after irradiation, but began to increase at 48 h and reached the highest level at 72 h after radiation (Fig. 1C). Taken together, the results indicated that 72 h after irradiation was an appropriate time to evaluate fibrotic phenotypes of LX-2 cell spheroids.

Down-regulation of circTUBD1 inhibited irradiation-induced LX-2 cell activation and fibrosis response

Knocking down circTUBD1 significantly reduced LX-2 cell viability, but LX-2 cells remained viable more than 6 days after irradiation (Fig. 2A, B). Compared with the nonirradiated group, irradiation significantly induced activation of LX-2 cells (e.g., increased α-SMA and expression of fibrosis-related molecules, including COL1A1, COL3A1, CTGF mRNA and protein. Down-regulation of circTUBD1 not only reduced LX-2 activity, but also significantly decreased the expression of fibrosis-related molecules (Fig. 2C, D). The relative expression of the proteins in Figure 2D is shown in Supplementary Figure 1A. We also performed immunofluorescence staining of the LX-2 spheroids, and the results were consistent with the results of qRT-PCR and western blotting (Fig. 2E). The relative quantitative fluorescence intensity in Figure 2E are shown in Supplementary Figure 1B.

MiR-203a-3p reversed the effect of circTUBD1 on the activation and profibrotic response of LX-2 cells

The prediction results from Circinteractome database indicated that circTUBD1 shared response elements for miR-203a-3p (Fig. 3A). Dual luciferase reporter assays indicated that compared with the miR-203a-3p negative control, mimics of miR-203a-3p significantly reduced the luciferase activity of a reporter containing the wild-type circTUBD1 sequence. However, it had no effect on the mutant circTUBD1 sequence (Fig. 3B, C). The results confirmed that circTUBD1 directly bound to miR-203a-3p. RNA pull-down assays further confirmed that miR-203a-3p was substantially enriched by the bio-circTUBD1 probe. Likewise, circTUBD1 was pulled down by the wild-type bio-miR-646 probe (Fig. 3D, E). We also examined how circTUBD1 regulated the radiation-induced activation and fibrosis response of LX-2 cells through interactions with miR-203a-3p. The results indicated that the level of miR-203a-3p or circTUBD1 was not significantly changed in LX-2 cells transfected with knockdown of circTUBD1 or miR-203a-3p mimics, compared with the corresponding control (Fig. 3F, G). Compared with the negative control, miR-203a-3p inhibitor aggravated radiation-induced activation and fibrosis of LX-2 cells, including the increasing of α-SMA, COL1A1, COL3A1, CTGF (Fig. 3H, I). The relative expression of proteins in Figure 3I are shown in Supplementary Figure 2. The suppression caused by silencing circTUBD1 was partially reduced by miR-203a-3p inhibitor. These results further revealed that circTUBD1 sponged miR-203a-3p to regulate the radiation-induced activation and fibrosis response of LX-2 cells.

MiR-203a-3p mediated circTUBD1 through SMAD3 to regulate the radiation-induced activation and fibrosis of LX-2 cells

The results of RNA sequencing suggested that the TGF-β signaling pathway ranked third among the top 15 enriched pathways and that the expression of SMAD3 was significantly downregulated after knockdown of circTUBD1 (Fig. 4A, B). To explore why knockdown of circTUBD1 resulted in the decrease of SMAD3, prediction database was used. The results of Targetscan indicated that there were multiple binding sites between miR-203a-3p and SMAD3-3′-untrasnlated region (UTR) (Fig. 4C). The dual luciferase assay findings revealed that miR-203a-3p mimics significantly reduced luciferase activity of the report vector containing wild-type of SMAD3 but had no significant effects on the mutant SMAD3 (Fig. 4D, E). These results showed that miR-203a-3p directly bound to SMAD3. To verify whether miR-203a-3p mediated the regulation of circTUBD1 through SMAD3, we transfected miR-203a-3p inhibitor into cells to knock down circTUBD1. The qRT-PCR and western blot results suggested that miR-203a-3p inhibitors partially reversed the inhibition effect of knocking down circTUBD1 on SMAD3, p-SMAD3, SMAD2, p-SMAD2, and TGF-β levels (Fig. 4F, G). The relative expression of the proteins in Figure 4G is shown in Supplementary Figure 3A. To examine whether SMAD3 was involved in radiation-induced activation and fibrosis response of LX-2 cells, we knocked down SMAD3. The results indicated that compared with the negative control, SMAD3 knockdown significantly inhibited radiation-induced activation and expression of fibrosis-related molecules in LX-2 cells, including the down-regulation of α-SMA, COL1A1, COL3A1, and CTGF. Knockdown of SMAD3 partially reversed the promotion effect of miR-203a-3p inhibitors on radiation-induced activation and fibrosis-related molecules of LX-2 cells (Fig. 4H–J). The relative expression of the proteins in Figure 4J is shown in Supplementary Figure 3B, C. The findings indicated that circTUBD was mediated by miR-203a-3p through SMAD3 to regulate the radiation-induced activation and fibrosis of LX-2 cells.

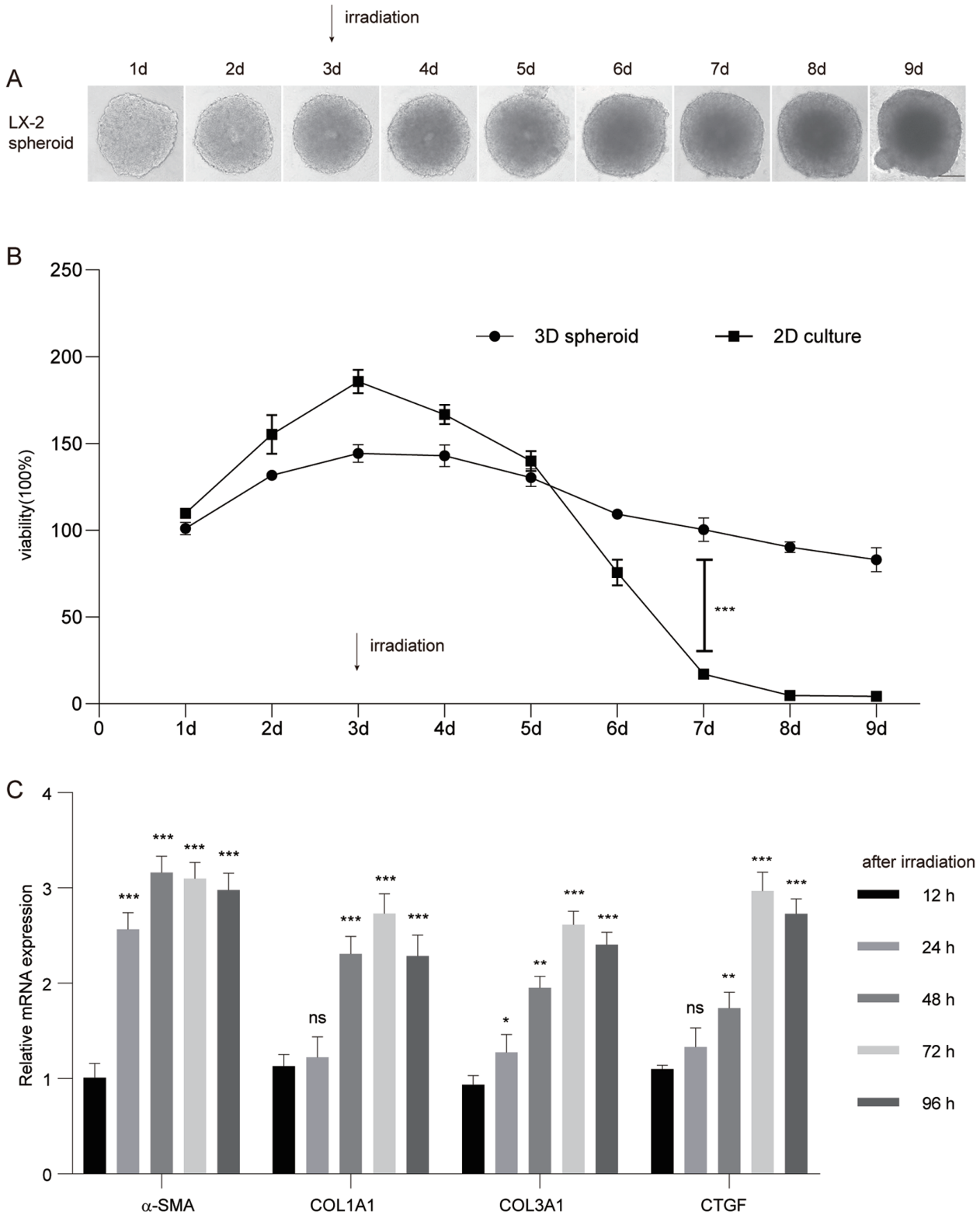

Fig. 1. Irradiation induced the activation and fibrosis response of the human hepatic stellate line LX-2 cells. (A) The representative morphology of LX-2 cells spheroids every day after irradiation (scale bar: 100 μm). (B) ATP level in LX-2 cells in 3D spheroid and 2D culture assayed by CellTiter-Glo Luminescent Cell Viability Assay Kits. (C) Expression of activation and fibrosis markers of LX-2 cells, including α-SMA, COL1A1, COL3A1, and CTGF assayed after irradiation by qRT-PCR. **p* <0.05, ***p*<0.01, ****p*<0.001. Bars are means ± SEM of at least three independent assays. 2D, two-dimensional; 3D, three-dimensional; COL1A1, collagen type I alpha 1; COL3A1, collagen type III alpha 1; CTGF, connective tissue growth factor. *ns*, not significant.

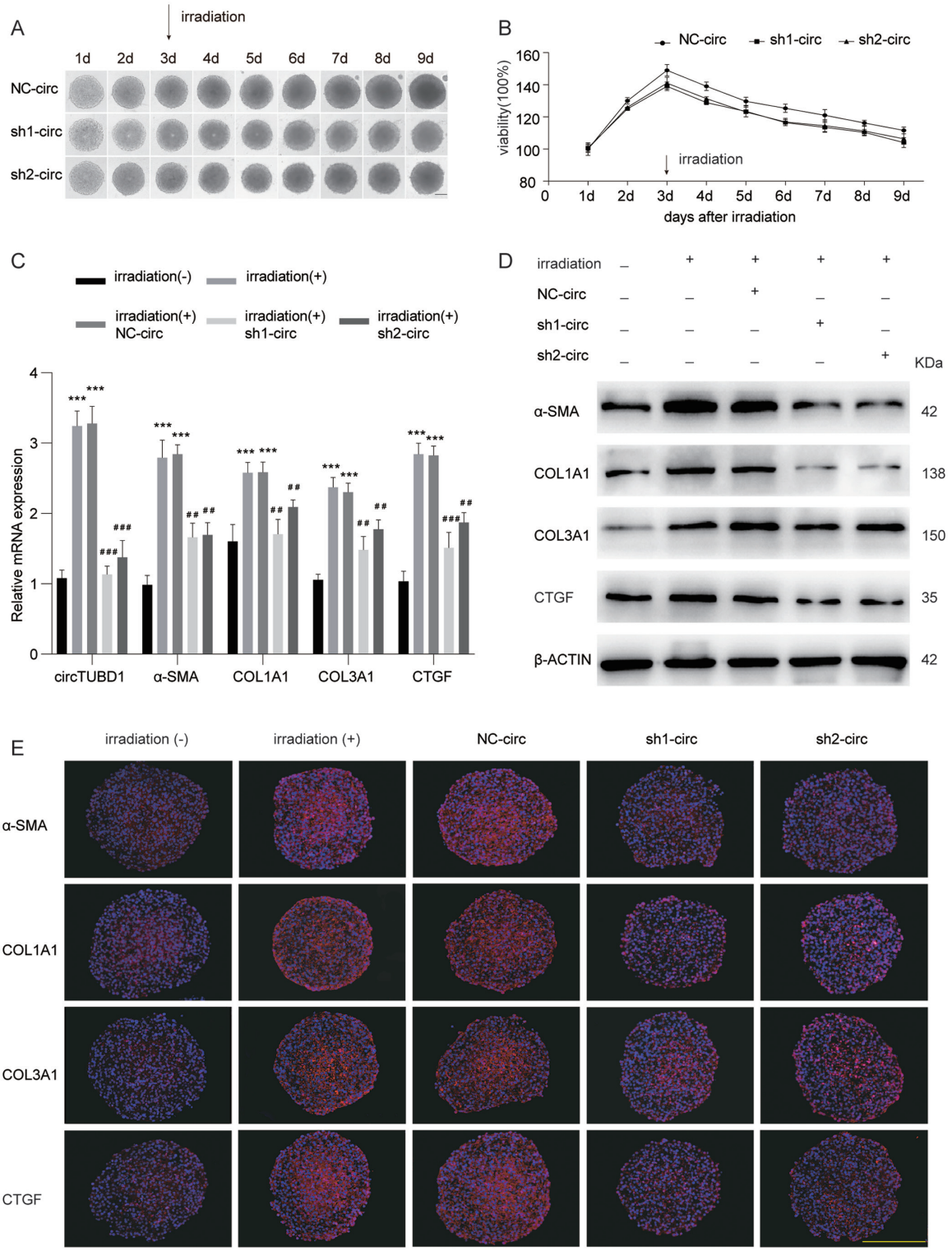

Fig. 2. Down-regulation of circTUBD1 suppressed the irradiation-induced activation and fibrosis response of LX-2 cells. (A, B) Representative images of 3D spheroids and the viability of transfected LX-2 cells with circTUBD1 knockdown every day after irradiation (scale bar: 100 μm). (C, D) qRT-PCR and western blot assays of circTUBD1, α-SMA, COL1A1, COL3A1, CTGF expression in transfected LX-2 cells with down-regulation of circTUBD1 and corresponding control 72 h after irradiation. (E) Representative images of immunofluorescence stained makers of activation and fibrosis molecules (CY3, red) in 3D spheroids of LX-2 cells with nucleic counterstained by DAPI (blue, scale bar: 200 μm). **p* vs. non-irradiation, $^{\#}p$ vs. NC-circ at 72 h after irradiation, ****p*<0.001. $^{\#\#}p$<0.01, $^{\#\#\#}p$<0.001. Bar are means ± SEM of at least three independent assays. NC-circ, negative control of circTUBD1; sh1-circ, short hairpin RNA 1 of circTUBD1; sh2-circ, short hairpin RNA 2 of circTUBD1. DAPI, 4′,6-diamidino-2-phenylindole; CY3, Cyanine3.

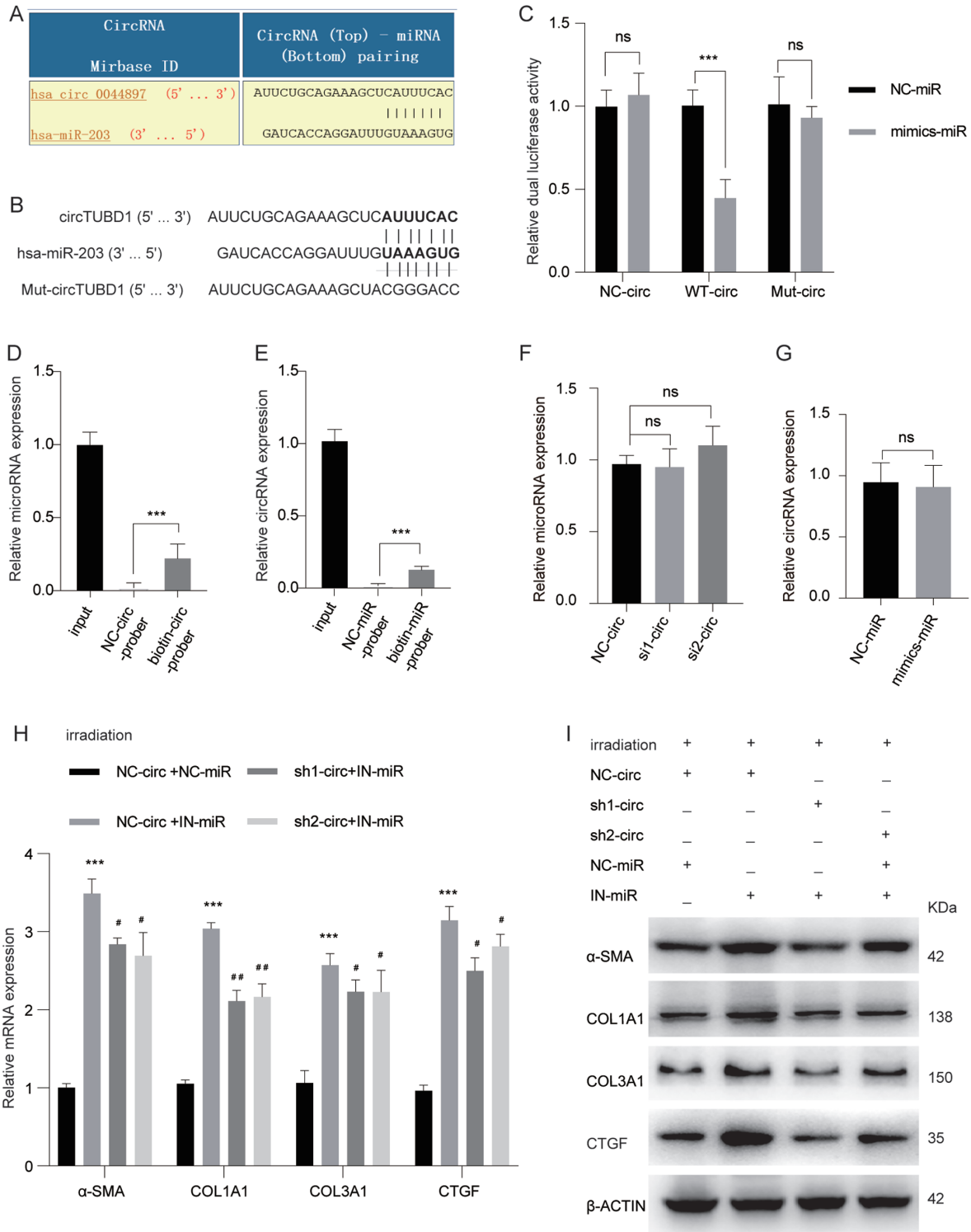

Fig. 3. MiR-203a-3p reverses the effect of circTUBD1 on the activation and profibrotic response of LX-2 cells. (A) Putative binding sites of circTUBD1 and microRNA response elements of miR-203a-3p predicted by Circinteractome. (B, C) Luciferase reporter assays in LX-2 cells co-transfected with wild-type, mutant circTUBD1, or negative control of luciferase vector and miR-203a-3p mimics, or negative control of miR-203a-3p mimics. (D, E) RNA pull-down assay followed by qRT-PCR of miR-203a-3p or circTUBD1 enriched with biotin-circTUBD1 probes or biotin-miR-203a-3p probes. (F, G) miR-203a-3p or circTUBD1 assayed by qRT-PCR in LX-2 cells transfected with knockdown of circTUBD1 or miR-203a-3p mimics. (H, I) α-SMA, COL1A1, COL3A1, CTGF in LX-2 expression assayed by qRT-PCR and western blot after co-transfection and knockdown of circTUBD1 with or without miR-203a-3p inhibitors or their negative controls. **p* vs. NC-circ and NC-miR, #*p* vs. NC-circ and IN-miR. *ns*: not significant, ****p*<0.001. #*p*<0.05, ##*p*<0.005. Bars are means ± SEM of at least three independent assays. NC-circ, negative control of circTUBD1; sh1-circ, sh1-TUBD1; sh2-circ, sh2-TUBD1; NC-miR, negative control of miR-203a-3p inhibitor; IN-miR, miR-203a-3p inhibitor; ns, not significant. WT, wild type; Mut, mutant.

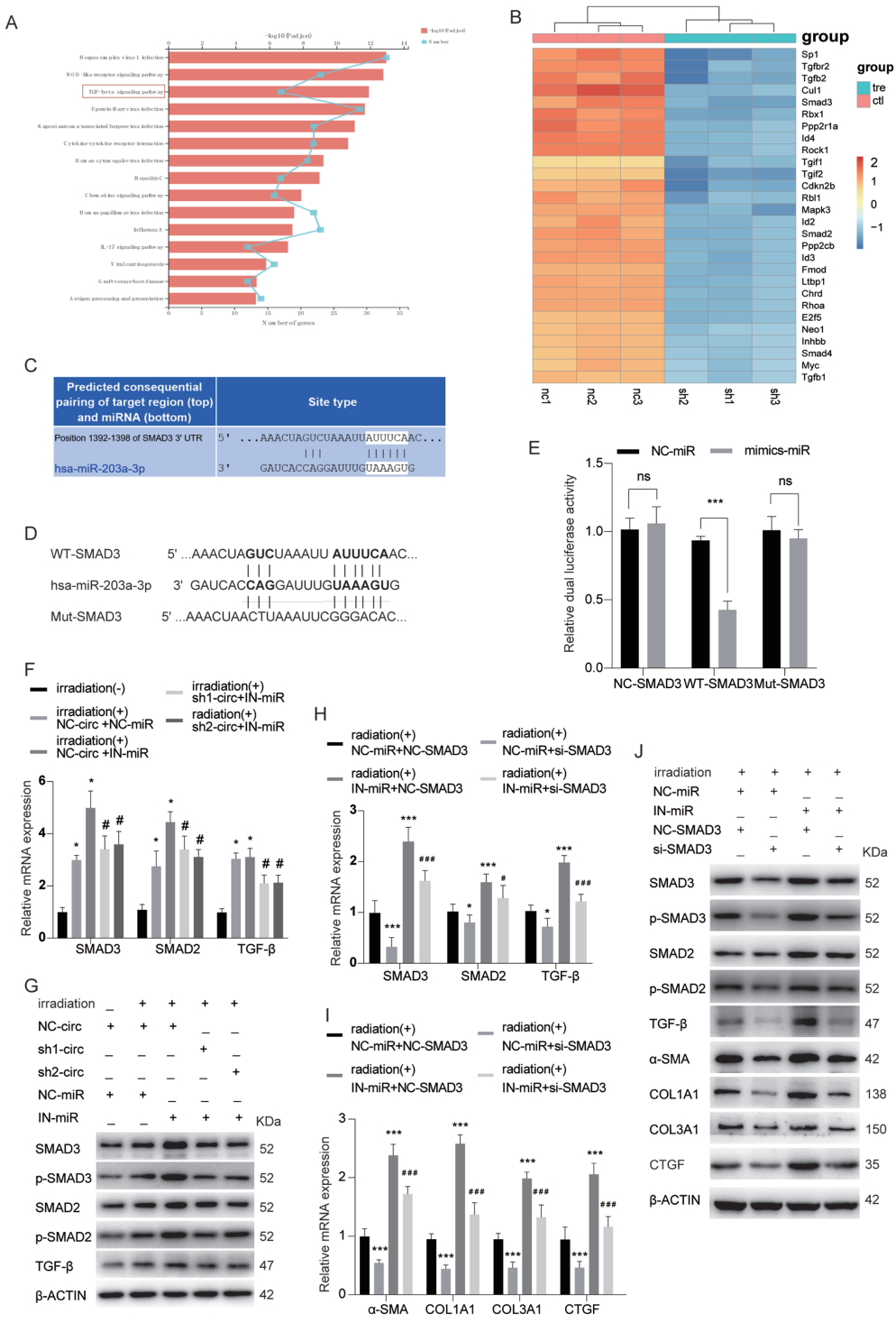

Fig. 4. MiR-203a-3p mediates the regulation of circTUBD1 on SMAD3. (A) TGF-β signaling pathway ranked third among the top 15 enriched pathways in the knockdown of circTUBD1 vs. control group by Kyoto Encyclopedia of Genes and Genomes pathway enrichment. (B) SMAD3 ranked fifth among the different genes contained in the TGF-β signaling pathway analyzed by cluster analysis and displayed in the heatmap. (p <0.05 vs. NC-circTUBD1, red: high, blue: low). (C) Binding sites of the seed region of miR-203a-3p and SMAD3 3′-UTR predicted by Targetscan. (D, E) Luciferase reporter assay in LX-2 cells co-transfected with wild-type, mutant SMAD3, or negative control with miR-203a-3p mimics or negative control. (F, G) Expression of SAMD3, p-SAMD3, SAMD2, p-SAMD2 and TGF-β protein assayed after irradiation by qRT-PCR and western blot after co-transfection with knockdown of circTUBD1 and miR-203a-3p inhibitor or control in LX-2 cells. (H–J) qRT-PCR and western blot assays of the expression of fibrosis markers and molecules at 72 h after irradiation by in LX-2 cells transfected with knockdown of SMAD3 or negative control with miR-203a-3p inhibitors. *p vs. NC-SMAD3 and NC-miR, $^{\#}p$ vs. IN-miR and NC-SMAD3 *ns*, not significant; *p<0.05; ***p<0.001; $^{\#}p$<0.05; $^{\#\#\#}p$<0.001. Bars are means ± SEM of at least three independent assays. NC-SMAD3, negative control of SMAD3; si-SMAD3, short interference RNA of SMAD3; NC-miR, negative control of miR-203a-3p inhibitor; IN-miR, miR-203a-3p inhibitor; ns, not significant.

CircTUBD1 was also be regulated by SMAD3 via a positive feed back

The predicted results from GTAR and JASPAR database revealed that SMAD3, as a transcription factor, possessed multiple transcription factor binding sites (TFBSs) in the TUBD1 promoter region (Fig. 5A, B). The results of the dual luciferase assay revealed that there were two effective TFBSs on the TUBD1 promoter region that bound to SMAD3 (Fig. 5C, D). To further examine how SMAD3 regulated circTUBD1, specific primers were designed to detect expression of TUBD1 pre-mRNA and TUBD1, and circTUBD1 mRNA (Fig. 6E). To explore the transcriptional regulation of SMAD3 on TUBD1, we performed ChIP assays using a mAb against SMAD3. ChIP-PCR analysis confirmed the occupancy of SAMD3 on the promoter of TUBD1 (Fig. 5F, G). Moreover, knockdown of SMAD3 significantly decreased TUBD1, pre-TUBD1, and circTUBD1 expression in LX-2 cells (Fig. 5H–J). Taken together, the findings suggest that SMAD3 was not only regulated by cirTUBD1, but it also regulated endogenous expression of circTUBD1.

Knockdown of circTUBD1 alleviated the progression of irradiation-induced liver fibrogenesis in vivo model

qRT-PCR and western blot assays found that irradiation induced up-regulation of α-SMA, COL1A1, COL3A1, and CTGF and knockdown of circTUBD1 partially alleviated the effect on the fibrosis makers (Fig. 6A, B). The relative expression of the proteins in Figure 6B are shown in Supplementary Figure 4. The RILF model was successfully constructed in C57BL/6 mice irradiated with 30 Gy X-ray in five fraction, manifested as the disruption of the regular lobular structure of liver, the extent of inflammatory cell infiltration (Fig. 6C), and excess collagen deposition around blood vessels 6 months after irradiation (Fig. 6 D, E). Notably, the results of immunohistochemistry confirmed that irradiation induced up-regulation of the above motioned fibrosis makers, and knockdown of circTUBD1 alleviated the fibrosis phenotype (Fig. 6F).

Discussion

RILF delayed post-irradiation damage to the liver that is inevitable and can be lethal.[2,3,5] In this study, it was found that knockdown of circTUBD1 alleviated radiation-induced activation and fibrosis response in 3D culture systems *in vitro* and in a RILF mouse model, including inhibition of α-SMA expression, reduction in the expression of the fibrosis-promoting molecules COL1A1, COL3A1, and CTGF in LX-2 cells treated with irradiation. The study results revealed that circTUBD1 regulated the activation and fibrosis response of LX-2 cells induced by irradiation through a circTUBD1/micro-203a-3p/Smad3 positive feedback loop.

To date, more than 380 cell lines have been established as 3D models and are used in drug toxicology studies, cancer research, and metabolomics research. The 3D culture system helps us understand complex cell physiology and cell function in response to stimuli in a condition closer to the *in vivo* environment. A previous study found that cells in 3D culture system enhanced extracellular matrix deposition and expression of biomarkers.[11] Through optimization of culture conditions, we successfully established an LX-2 cell 3D spheroid culture system as an *in vitro* model for the study of the mechanism of RILF. Our results confirmed that viability of the LX-2 cells was maintained longer after irradiation in the 3D spheroid system. More important, we discovered that the increases in α-SMA, COL1A1, COL3A1, and CTGF induced by irradiation were significant higher in the 3D model than in 2D culture. It is possible that LX-2 cells were auto-activated in 2D culture. It was also found that irradiation induced significant increases in the expression of TGF-β and SMAD3 in activated LX-2 cells. The results are consistent with those of previous studies.[16,17] Taken together, our results and those of previous studies confirm that the 3D spheroid system is a useful *in vitro* model that has advantages over 2D culture for the study of chronic liver diseases.[11]

Many small RNAs have been identified as being involved in regulation of disease.[18] Different small RNAs are multidimensional and have significantly different biological activity. Dysregulation of small RNAs, like miRNAs and circRNAs, contributes to regulation of the progression of hepatic fibrosis by targeting mRNAs.[19] It has been reported that circRNA_000203 enhanced the expression of fibrosis-associated genes by derepressing targets of miR-26b-5p, Col1a2 and CTGF, in cardiac fibroblasts.[20] In this study, we showed that irradiation induced a significant increase of circTUBD1 in LX-2 cells. Knockdown of circTUBD1 inhibited HSC activation and profibrotic molecules, such as α-SMA, COL1A1, COL3A1, and CTGF. The results indicated that circTUBD1 was involved in radiation-induced LX-2 cell activation and profibrotic response. Study findings suggest that miR-203a-3p also inhibits HSC proliferation and attenuates liver fibrosis in mice via modulation of the p66Shc/β-catenin pathway induced by CCl4.[21] We found that miR-203a-3p inhibitor significantly promoted the radiation-induced activation and fibrosis of LX-2 cells. Our results, which were partially consistent with previous studies, confirmed that miR-203a-3p inhibited liver fibrosis. We also confirmed that knockdown of circTUBD1 could reverse the promotion effect of miR-203a-3p inhibitors on the radiation-induced activation and fibrosis of LX-2 cells. Our previous studies showed that LX-2 cells immediately secreted large amounts of proinflammatory cytokines, including interleukin (IL)-1β, IL6, and tumor necrosis factor alpha (TNF-α) 24 h after irradiation, which regulated by circTUBD1/miR-146a-5p/TLR4 pathway.[22] In this study, we found that HSCs began to synthesize a large amount of collagen at 48 h after radiation. Our previous work and the study results together suggest that radiation-induced activation of HSCs not only promote the secretion of inflammatory factors in the early stage but also promote the synthesis of fibrosis in the late stage through different signaling pathways.

The TGF-β/SMAD3 signaling pathway is an important mediator during regulation of responses to radiation-induced acute or chronic injury in the liver.[16,17] Experimental and clinical studies have found that the TGF-β/SMAD3 signaling pathway promotes a radiation dose-dependent increase in the inhibition of TGF-β/SMAD3 that reduces post-irradiation liver fibrosis in animals. Our LX-2 cell spheroid model also revealed an irradiation-induced activation of the TGF-β/SMAD3 signaling pathway. Anti-TGF-β therapy is a potential therapeutic strategy against RILF. Nevertheless, direct antagonization of TGF-β activity to reduce RILF will be a challenge because TGF-β is active in maintaining normal physiological activities in various cells of the liver. Therefore, the therapeutic approach of direct targeting of TGF-β to inhibit liver fibrosis would introduce unavoidable side effects. But we cannot completely negate the role of the TGF-β signaling pathway, as it may be a potential strategy to alleviate RILF by inhibiting downstream regulators like SMAD2 and SMAD3. Our previous study using circRNA microarrays revealed that circTUBD1 expression in LX-2 cells was specifically and significantly increased when induced by irradiation,[15] and Kyoto Encyclopedia of Genes and Genomes results suggested that the TGF-β signaling pathway ranked third among all pathways,

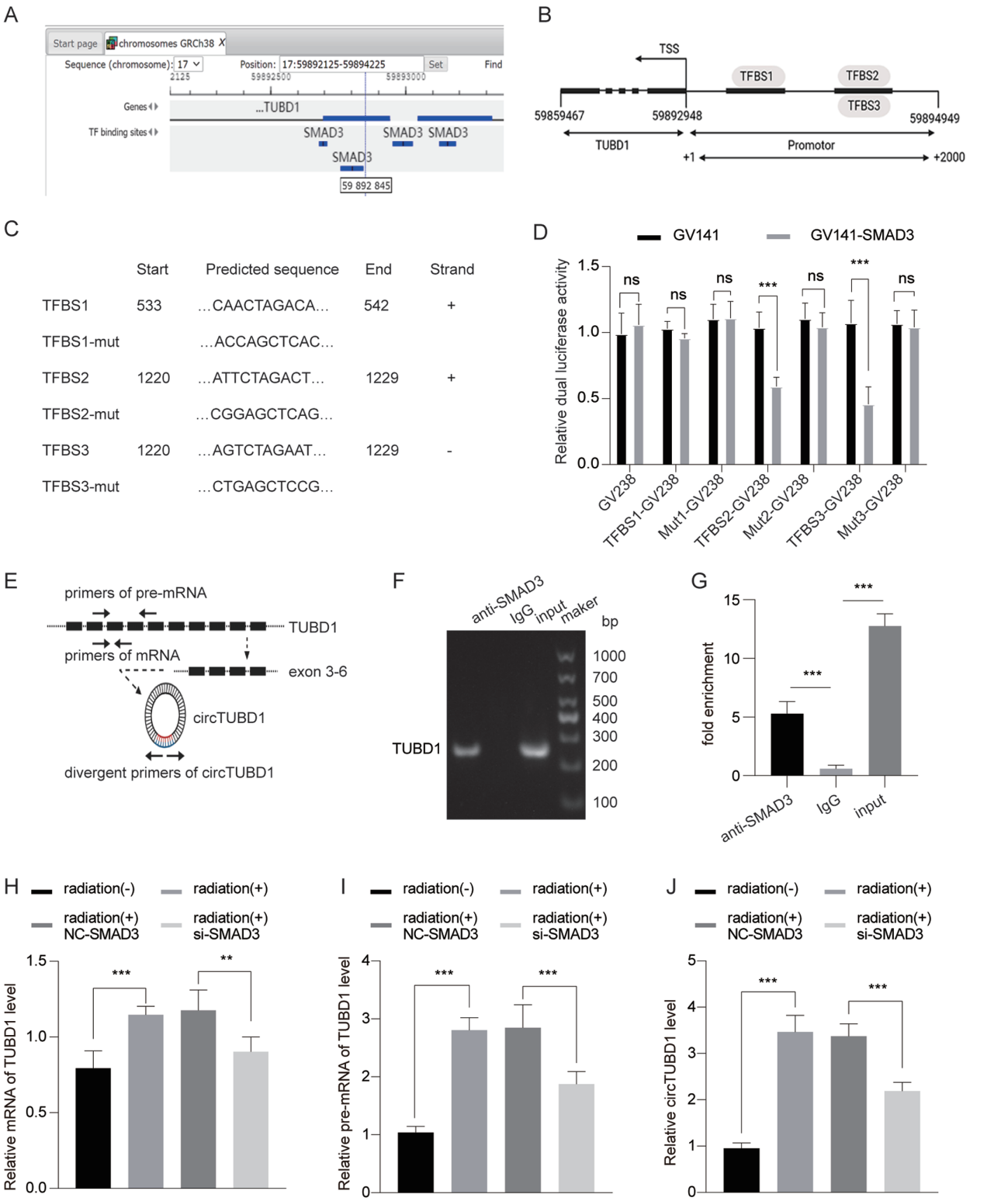

Fig. 5. SMAD3 regulates circTUBD1 by targeting the pre-mRNA of TUBD1. (A, B) TFBSs in the promoter region of TUBD1 for SMAD3 predicted by GTAR and JASPA data. (C, D) Luciferase reporter assay in LX-2 cells co-transfected with wild-type, mutant TFBS of TUBD1 in GV238 vector, or negative control with SMAD3 over-expression (GV141-SMAD3) or negative control. (E) Diagram of the specific primers designed to detect pre-mRNA of TUBD1, mRNA of TUBD1, and circTUBD1. (F, G) ChIP assay of the TUBD1 promoter using antibodies against SMAD3 in LX-2 cells and analyzed by PCR. (H, I) Expression of mRNA, pre-mRNA of TUBD1, and circTUBD1 in LX-2 cells by qRT-PCR. $^{**}p<0.01$, $^{***}p<0.001$. Bars are means ± SEM of at least three independent assays. NC-SMAD3, negative control of SMAD3; si-SMAD3, short interference RNA of SMAD3; NC-miR, negative control of miR-203a-3p inhibitor; IN-miR, miR-203a-3p inhibitor; ns, not significant.

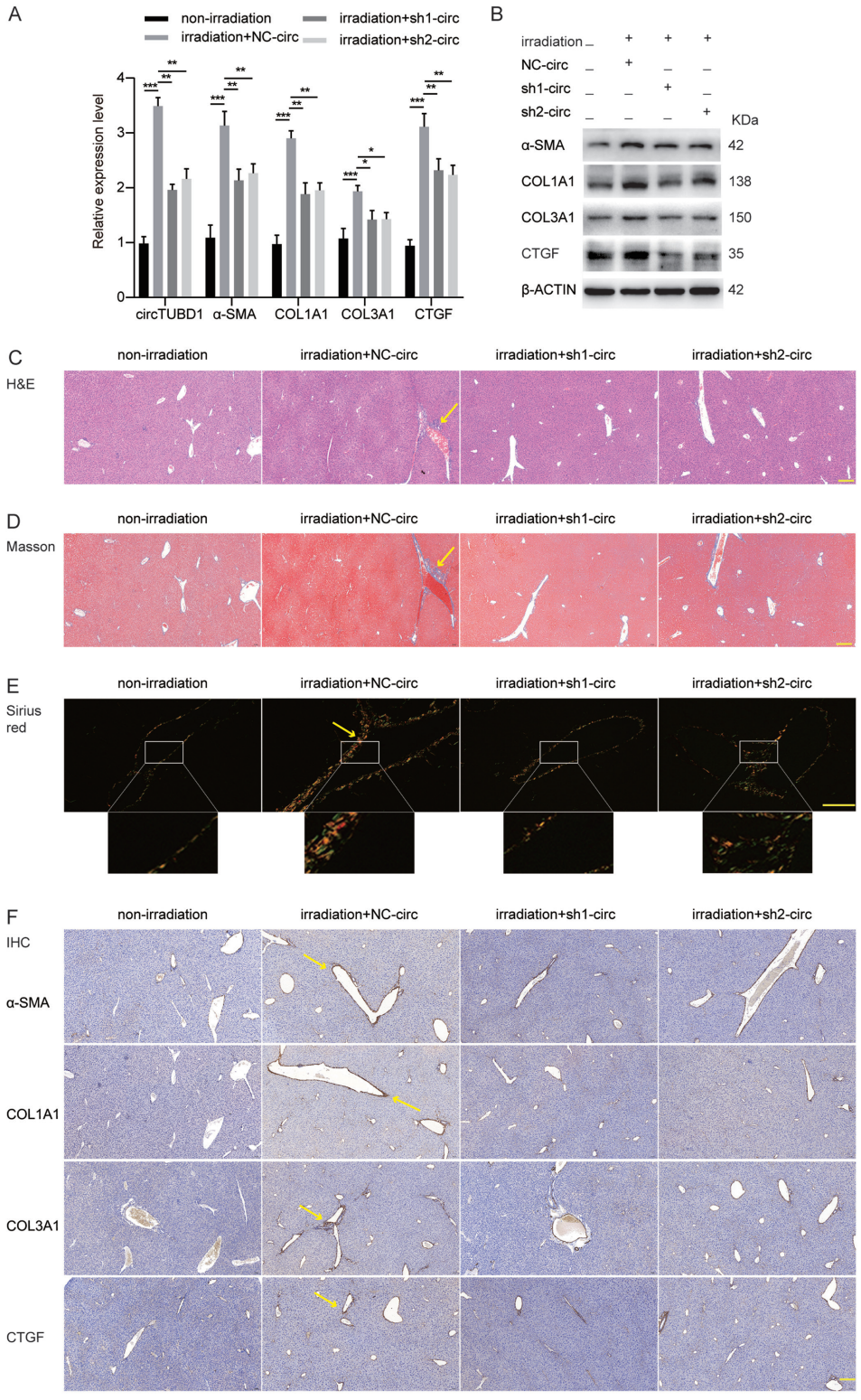

Fig. 6. Knockdown of circTUBD1 alleviated irradiation-induced liver fibrogenesis *in vivo* model. (A, B) qRT-PCR and Western blot assays of the relative expression of activation and fibrosis markers α-SMA, COL1A1, COL3A1, and CTGF in mice at 6 months after irradiation. (C) Hematoxylin and eosin stained tissue showed irradiation-induced disruption of the regular lobular structure of the liver and the infiltration of inflammatory cells (yellow arrow); scale bar: 500 μm. (D, E) Masson and Sirius red staining show excess collagen deposition around the vessel 6 months after irradiation (yellow arrow); scale bar: 500 μm). (F) Immunohistochemistry shows that knockdown of circTUBD1 reduced the fibrosis phenotype and fibrosis makers (α-SMA, COL1A1, COL3A1, and CTGF) induced by irradiation. **p* <0.05, ***p*<0.01, ****p*<0.001. Bar represent means ± SEM of at least three independent assays. NC-circ, negative control of circTUBD1; sh1-circ, sh1-TUBD1; sh2-circ, sh2-TUBD1.

with significant differences after knockdown of circTUBD1. The result implied that altering circTUBD1 significantly affected the TGF-β pathway. We further confirmed that, as a sponge of miR-203a-3p, circTUBD1 was involved in regulation of the radiation-induced LX-2 cell profibrotic response through SMAD3. Although the general components of TGF-β/SMADs signaling is now understood, the core issue of how to control TGF-β/SMAD signaling in context remains unclear.[23,24] It has been reported that SMAD3 mediates the constitutive active loop between lncRNA PCAT7 and the TGF-β signaling pathway to promote cancer metastasis.[25] However, the central question of how the TGF-β/SMAD feedback model exerts its versatile and context-dependent functions in liver fibrosis is unclear. In this study, we found that the expression level of circTUBD1 changed after knockdown of SMAD3. Using different methods, we confirmed that SMAD3 was not only regulated by cirTUBD1, it also regulated the endogenous expression of circTUBD1 and forms a positive feedback. The feedback mode helps to adjust the signal strength more effectively.

In previous studies, RILF models were established by irradiation whole liver.[1,16] To exclude individual differences and better simulate focal radiation in clinical, we irradiated only the left liver of mice with X-rays. Compared with the right liver, the left liver manifested infiltration of a number of inflammatory cells infiltrate around blood vessels and vascular and interstitial congestion at early stages. The regular lobular structure was partially disrupted, and excess collagen was deposited in the interstitium, especially around the vessels. Notably, we observed that irradiation induced migration of HSCs to vascular spaces from the subendothelial space of Disse, which further confirmed that HSCs have an important role in irradiation-induced collagen deposition around the vessels. These results implied that knockdown of circTUBD1 inhibited the cascade reaction induced by the circTUBD1/micro-203a-3p/Smad3 positive feedback loop and reduced collagen secretion from HSCs, may be a potential strategy to alleviate the RILF.

Conclusion

This study clarified the activities and mechanism of circTUBD1 in the process of RILF through a circTUBD1/miR-203a-3p/SMAD3 positive feedback loop by 3D model *in vitro* and RILF model in vivo. Knockdown of the specific circTUBD1 may be a potential strategy for effective prevention of RILF.

Funding

This work was supported by National Natural Science Foundation of China (Grant Nos. 81773220 and 82003225). Shanghai Sailing Program (Grant No. 20YF1405500), the Youth Programme of Zhongshan Hospital, Fudan University (Grant No. 2020ZSQN24).

Conflict of interest

The authors have no conflict of interests related to this publication.

Author contributions

Study conception and design (ZCZ), data acquisition (HN, LZ), data analysis and interpretation (BW, GCZ), manuscript drafting (HN), manuscript revision for important intellectual content (JL, ZFW, SSD), and administrative, technical, material support, and study supervision (ZCZ).

Ethical statement

The study was approved by the Zhongshan Hospital Research Ethics Committee.

Data sharing statement

Research data will be shared upon reasonable request directed to the corresponding author.

References

[1] Koay EJ, Owen D, Das P. Radiation-Induced Liver Disease and Modern Radiotherapy. Semin Radiat Oncol 2018;28(4):321–331. doi:10.1016/j.semradonc.2018.06.007, PMID:30309642.
[2] Straub JM, New J, Hamilton CD, Lominska C, Shnayder Y, Thomas SM. Radiation-induced fibrosis: mechanisms and implications for therapy. J Cancer Res Clin Oncol 2015;141(11):1985–1994. doi:10.1007/s00432-015-1974-6, PMID:25910988.
[3] Benson R, Madan R, Kilambi R, Chander S. Radiation induced liver disease: A clinical update. J Egypt Natl Canc Inst 2016;28(1):7–11. doi:10.1016/j.jnci.2015.08.001, PMID:26300327.
[4] Dawson LA, Normolle D, Balter JM, McGinn CJ, Lawrence TS, Ten Haken RK. Analysis of radiation-induced liver disease using the Lyman NTCP model. Int J Radiat Oncol Biol Phys 2002;53(4):810–821. doi:10.1016/s0360-3016(02)02846-8, PMID:12095546.
[5] Toesca DAS, Ibragimov B, Koong AJ, Xing L, Koong AC, Chang DT. Strategies for prediction and mitigation of radiation-induced liver toxicity. J Radiat Res 2018;59(suppl_1):i40–i49. doi:10.1093/jrr/rrx104, PMID:29432550.
[6] Chou CH, Chen PJ, Lee PH, Cheng AL, Hsu HC, Cheng JC. Radiation-induced hepatitis B virus reactivation in liver mediated by the bystander effect from irradiated endothelial cells. Clin Cancer Res 2007;13(3):851–857. doi:10.1158/1078-0432.Ccr-06-2459, PMID:17289877.
[7] van Grunsven LA. 3D in vitro models of liver fibrosis. Adv Drug Deliv Rev 2017;121:133–146. doi:10.1016/j.addr.2017.07.004, PMID:28697953.
[8] Puche JE, Saiman Y, Friedman SL. Hepatic stellate cells and liver fibrosis. Compr Physiol 2013;3(4):1473–1492. doi:10.1002/cphy.c120035, PMID:24265236.
[9] Pingitore P, Sasidharan K, Ekstrand M, Prill S, Lindén D, Romeo S. Human Multilineage 3D Spheroids as a Model of Liver Steatosis and Fibrosis. Int J Mol Sci 2019;20(7):1629. doi:10.3390/ijms20071629, PMID:30986904.
[10] Coll M, Perea L, Boon R, Leite SB, Vallverdú J, Mannaerts I, *et al*. Generation of Hepatic Stellate Cells from Human Pluripotent Stem Cells Enables In Vitro Modeling of Liver Fibrosis. Cell Stem Cell 2018;23(1):101–113.e107. doi:10.1016/j.stem.2018.05.027, PMID:30049452.
[11] Ravi M, Paramesh V, Kaviya SR, Anuradha E, Solomon FD. 3D cell culture systems: advantages and applications. J Cell Physiol 2015;230(1):16–26. doi:10.1002/jcp.24683, PMID:24912145.
[12] Zhang F, Zhang R, Zhang X, Wu Y, Li X, Zhang S, *et al*. Comprehensive analysis of circRNA expression pattern and circRNA-miRNA-mRNA network in the pathogenesis of atherosclerosis in rabbits. Aging 2018;10(9):2266–2283. doi:10.18632/aging.101541, PMID:30187887.
[13] Meng J, Chen S, Han JX, Qian B, Wang XR, Zhong WL, *et al*. Twist1 Regulates Vimentin through Cul2 Circular RNA to Promote EMT in Hepatocellular Carcinoma. Cancer Res 2018;78(15):4150–4162. doi:10.1158/0008-5472.Can-17-3009, PMID:29844124.
[14] Ji D, Chen GF, Wang JC, Ji SH, Wu XW, Lu XJ, *et al*. Hsa_circ_0070963 inhibits liver fibrosis via regulation of miR-223-3p and LEMD3. Aging 2020;12(2):1643–1655. doi:10.18632/aging.102705, PMID:32003753.
[15] Chen Y, Yuan B, Wu Z, Dong Y, Zhang L, Zeng Z. Microarray profiling of circular RNAs and the potential regulatory role of hsa_circ_0071410 in the activated human hepatic stellate cell induced by irradiation. Gene 2017;629:35–42. doi:10.1016/j.gene.2017.07.078, PMID:28774651.
[16] Kumar D, Yalamanchali S, New J, Parsel S, New N, Holcomb A, *et al*. Development and Characterization of an In Vitro Model for Radiation-Induced Fibrosis. Radiat Res 2018;189(3):326–336. doi:10.1667/rr14926.1, PMID:29351058.
[17] Hu Z, Qin F, Gao S, Zhen Y, Huang D, Dong L. Paeoniflorin exerts protective effect on radiation-induced hepatic fibrosis in rats via TGF-β1/Smads signaling pathway. Am J Transl Res 2018;10(3):1012–1021. PMID:29636890.
[18] Barcena-Varela M, Colyn L, Fernandez-Barrena MG. Epigenetic Mechanisms in Hepatic Stellate Cell Activation During Liver Fibrosis and Carcinogenesis. Int J Mol Sci 2019;20(10):2507. doi:10.3390/ijms20102507, PMID:31117267.
[19] Kristensen LS, Andersen MS, Stagsted LVW, Ebbesen KK, Hansen TB, Kjems J. The biogenesis, biology and characterization of circular RNAs. Nat Rev Genet 2019;20(11):675–691. doi:10.1038/s41576-019-0158-7, PMID:31395983.
[20] Tang CM, Zhang M, Huang L, Hu ZQ, Zhu JN, Xiao Z, *et al*. CircRNA_000203

enhances the expression of fibrosis-associated genes by derepressing targets of miR-26b-5p, Col1a2 and CTGF, in cardiac fibroblasts. Sci Rep 2017;7:40342. doi:10.1038/srep40342, PMID:28079129.
[21] Wang Z, Zhao Y, Zhao H, Zhou J, Feng D, Tang F, *et al*. Inhibition of p66Shc Oxidative Signaling via CA-Induced Upregulation of miR-203a-3p Alleviates Liver Fibrosis Progression. Mol Ther Nucleic Acids 2020;21:751–763. doi:10.1016/j.omtn.2020.07.013, PMID:32781430.
[22] Niu H, Zhang L, Chen YH, Yuan BY, Wu ZF, Cheng JC, *et al*. Circular RNA TUBD1 Acts as the miR-146a-5p Sponge to Affect the Viability and Pro-Inflammatory Cytokine Production of LX-2 Cells through the TLR4 Pathway. Radiat Res 2020;193(4):383–393. doi:10.1667/rr15550.1, PMID:32097101.
[23] Hu HH, Chen DQ, Wang YN, Feng YL, Cao G, Vaziri ND, *et al*. New insights into TGF-β/Smad signaling in tissue fibrosis. Chem Biol Interact 2018;292:76–83. doi:10.1016/j.cbi.2018.07.008, PMID:30017632.
[24] Xu F, Liu C, Zhou D, Zhang L. TGF-β/SMAD Pathway and Its Regulation in Hepatic Fibrosis. J Histochem Cytochem 2016;64(3):157–167. doi:10.1369/0022155415627681, PMID:26747705.
[25] Lang C, Dai Y, Wu Z, Yang Q, He S, Zhang X, *et al*. SMAD3/SP1 complex-mediated constitutive active loop between lncRNA PCAT7 and TGF-β signaling promotes prostate cancer bone metastasis. Mol Oncol 2020;14(4):808–828. doi:10.1002/1878-0261.12634, PMID:31925912.